C-band circular corrugated horn design

L. Cresci[1], P. Curioni[1], V. Natale[1], R. Nesti[1], A. Orfei[2], D. Panella[1], J. Roda[2]

[1] INAF-Arcetri Astrophysical Observatory, Largo E. Fermi 5, I-50125 Florence (Italy)
[2] INAF- Istituto di Radioastronomia, Via P. Gobetti 101, I-40129 Bologna (Italy)

Arcetri Technical Report N° 4/2010
Firenze 2010

ISTITUTO NAZIONALE DI ASTROFISICA
OSSERVATORIO ASTROFISICO DI ARCETRI
L.GO E. FERMI, 5, 50125 – FIRENZE

Abstract

In this report the authors present the design of a circular corrugated horn for a radio astronomy receiver operating in the C band, from 5.7GHz to 7.7GHz. The horn was made in two parts that can be combined in order to match the requirements of two different optical systems: one is the Gregorian configuration of the Sardinia Radio Telescope where the feed will operate and the other is the Cassegrain configuration of the Medicina Radio Telescope where the whole receiver will be first tested. To provide optimum sensitivity, a parametric study of the edge taper to maximize the antenna gain over system temperature was made in the case of the Sardinia Radio Telescope.

1 Introduction

Radio astronomy receivers make large use of circular corrugated horns as feeds for large reflector antennas, especially when high performances are required. Circular corrugated horns [1] show high beam symmetry, high return loss, low side lobe levels and low cross polarization over wide bands.

The design of a circular corrugated horn for a C band (5.7GHz – 7.7GHz) radio astronomy receiver is here presented. An interesting aspect is that this receiver has to operate on the new Sardinia Radio Telescope (SRT) [2] and to be tested on the antenna of Medicina (MED) [3]. Differently from all the other receiver subsystems, the feed is affected by the antenna optics and thus two circular corrugated horns are, in principle, required for optimum coupling with the mirrors of the two radio telescopes.

Almost the entire world of reflector antenna configurations are to be taken into account in the design of the horn and, furthermore, some modern and practical solutions are implemented in the two radio telescopes: in the design of the horn for the third focus of the SRT gregorian antenna and for the secondary focus of the MED cassegrain antenna, it has to be considered, at the same time, third focusing with a mirror pair and gregorian and cassegrain dual reflector configurations. It seems thus useful to recall at the beginning some well known and general concepts like *focal length*, *focal ratio* and *feed tapering*, which are commonly used to characterize any kind of optics.

This theoretical discussion is followed by the description of the horn design, trying to put in evidence the use of *focal length*, *focal ratio* and *feed tapering* as design parameters for feeds coupled to reflector antennas.

The last part is concerned with fabrication aspects and electromagnetic tests.

2 The Optics of the SRT and MED antennas

The law governing the mathematical transformation of the *focal ratio* along a chain of mirrors used as re-focusing elements is first discussed and finally the data of the SRT and MED optics, used as specifications for the horn design, are summarized. Consider first the MED antenna optics, a dual reflector system with a hyperboloid that re-focuses the EM radiation coming from a large collecting area paraboloid, forming a cassegrain configuration and sketched in Fig. 1a. The paraboloid as a curve is characterized by its *focal length F*, the distance between the focus and the vertex; the paraboloid as a reflector antenna is characterized by its *focal ratio F/D*, the ratio between the *focal length F* and the aperture diameter *D*. As shown in the Appendices, the *focal ratio* and the *taper angle* Ψ (the angle from the edges to the vertex of the paraboloid as seen from the paraboloid focus) are related by (12). The concept of *focal ratio* can also be extended to a receiver placed in the secondary focus of the antenna, that is the focus of the ellipsoid not shared with the paraboloid. As an important result of the discussion in Appendices, it was found (14) and, noticing that, in the case of Fig 1a, $\phi = \phi_1$ and $\Psi = \phi_2$, it follows that

$$\tan\left(\frac{\phi}{2}\right) = \frac{D}{4F\frac{F_1}{F_2}} = \frac{D}{4F_{II}} \tag{1}$$

Thus a receiver in the secondary focus sees an equivalent paraboloid [4] with the same diameter D, subtended by the angle ϕ. The equivalent optics can thus be characterized by an effective *focal ratio* F_{II}/D, with the effective *focal length* F_{II} given by

$$F_{II} = F\frac{F_1}{F_2} \tag{2}$$

The same considerations and the same relation (2) holds also in the case of the gregorian configuration in Fig. 1b.

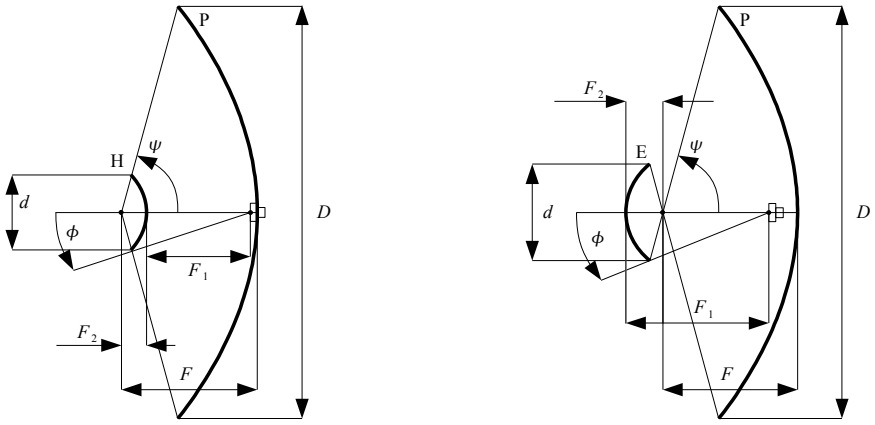

Fig. 1: Sketch of dual reflector antenna configurations: in the cassegrain (a) the hyperboloid H re-focuses the EM field at a distance F_1+F_2 from the paraboloid focus; in the gregorian (b) the ellipsoid E re-focuses the EM field at a distance F_1-F_2 from the paraboloid focus.

In the case of SRT the matter is more complicated since the receiver is not placed in the gregorian focus, but in a third focus, formed by a pair of ellipsoids on the backside of the paraboloid. From the above considerations on the gregorian and cassegrain dual reflector configurations, it can be noticed that the ellipsoid (and the hyperboloid as well) behaves like a *focal length* transformer ruled by the factor F_1/F_2; F_1 is the *focal length* to the secondary focus where the radiation scattered by the secondary mirror converges and F_2 is the *focal length* to the prime focus which is coincident with the paraboloidal main mirror focus. There is a little difference in the behaviour of the two kinds of secondary mirrors as regards this last focus: in the ellipsoid case, the incident radiation to the secondary scatterer really comes from the prime focus like it was a point source; in the case of the hyperboloid, the secondary scatterer shields the prime focus which can be thus considered only as a virtual point source.

Suppose now to have a second ellipsoidal mirror with one focus on the secondary focus and the other focus on a third point (third focus). The radiation will be re-focused on the third focus and, if we name F_{11} and F_{12} the *focal length* of the second ellipsoid to, respectively, the third and the secondary focus, it can be written

$$F_{III} = F_{II}\frac{F_{11}}{F_{12}} \tag{3}$$

were F_{III} is the equivalent *focal length* of the equivalent paraboloid as seen from the third focus. Adding more re-focusing ellipsoids the diameter D of the equivalent paraboloid will be kept unchanged, while the equivalent *focal length* will iteratively follow the rule in (3).

What is named third focus in the SRT antenna is the one re-focused by means of a pair of ellipsoids and thus the real full formula is

$$\tan\left(\frac{\phi'}{2}\right) = \frac{D}{4F\dfrac{F_1}{F_2}\dfrac{F_{11}}{F_{12}}\dfrac{F_{21}}{F_{22}}} = \frac{D}{4F_{III}} \tag{4}$$

where the further contribution of a third ellipsoid with *focal lengths* F_{21} and F_{22} is included. The effective *focal length* at the third focus becomes F_{III}, corresponding to a feed taper angle ϕ' according to (4).

A summary of the optical parameters of the SRT and MED antennas is given in Table I.

Table I

SRT and MED optics				
	SRT		MED	
Parameter	[m]	Effective focal ratio	[m]	Effective focal ratio
Primary diameter (D)	64		32	
Secondary diameter (d)	7.9		3.2	
Primary focal length (F)	21	F/D: 0.328	10.26	F/D: 0.32
Focal length F_1	20.32		9.07	
Focal length F_2	2.85	F_{II}/D: 2.34	0.96	F_{II}/D: 3.029
Focal length F_{11}	2.4		n.a.	
Focal length F_{12}	7		n.a.	
Focal length F_{21}	3.6		n.a.	
Focal length F_{22}	2.1	F_{III}/D: 1.375	n.a.	

3 Gain and system temperature model for the SRT antenna

In the optimization of the performances of a large reflector antenna used in radio astronomy applications, the key parameter is the ratio between the antenna gain G and the system temperature T_{sys}. This figure has to be maximized for best sensitivity [5] and it is strictly related to the edge taper of the feed. Through the illumination efficiency and the spillover [6], trading each other off in improving the antenna gain and driving the environmental noise temperature inside the receiver, the edge taper directly affects both the gain and the system temperature: both of these figures increase with the edge taper and, in practice, an accurate electromagnetic study of each antenna is needed to find its optimum edge taper maximizing the G/T_{sys} figure.

In the case of the SRT the configuration is shown in Fig. 2.

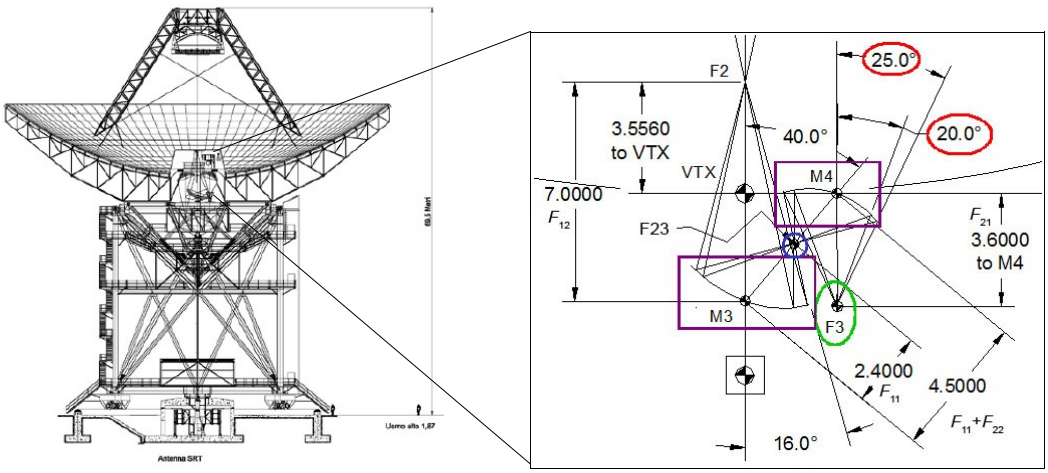

Fig. 2: SRT sketch (left) with a geometrical zoom of the beam path to the third focus (right).

The feed is hosted inside a vertex room where the beam is focused on the so called *beam waveguide focus* (BWF) by means of two ellipsoidal mirrors M3 and M4. The focal points are F2 (the gregorian secondary focus), F23 (an intermediate focus) and F3, which is the BWF. From this focus, two angles are highlighted in Fig. 2: a 25° angle to the

real edges of the M4 mirror and a 20° angle, corresponding to the edges of the secondary mirror in the geometrical optics path from F3. The 5° extra angle helps to shield the vertex room 300K radiation, otherwise entering the receiver through the tail of the main beam of the feed. Discussing the edge taper it is thus correct to refer to the lower 20° angle.

The antenna gain is easily obtained as the maximum radiation intensity [6] of the beam pattern once input unit power is provided to the feed; in our case it is a direct output of our computational software tool. As regards the system temperature a few more words are worthwhile to be spent. The system temperature can be seen as the sum of the antenna temperature T_a entering the receiver through the feed beam and the equivalent receiver temperature T_r taking into account the noise temperature introduced by the other parts in the receiver chain [7] and thus

$$T_{sys} = T_a + T_r \tag{5}$$

In this case an accurate estimate of the equivalent receiver temperature is T_r = 13K. The antenna temperature has three different contributions, as shown in Fig. 3. Two of them are collected by the main and the subreflector: the sky temperature T_{Sky}, coming from the sky and the earth temperature T_{Earth}, coming from the earth. The third enters directly through the feed due to spillover effects on the fourth mirror M4 and is generated by the vertex room, uniformly hot at T_{B_BWG} = 290K (BWG is for Beam WaveGuide).

Fig. 3: Contributions to the SRT antenna temperature: sky and earth (left) and beam waveguide room (right).

The sky and the earth temperature contributions are calculated as a weighted integral involving the antenna pattern and the sky brilliance temperature distribution T_B, according to data and models discussed in [8]. Referring to the sketch in the left side of Fig. 4, naming G the normalized gain pattern of the antenna, (θ_0, ϕ_0) the direction pointed by the antenna and (θ, ϕ) the co-ordinates of the generic temperature point source P in the sky, the antenna temperature due to the sky and the earth can be calculated as:

$$T_a'(\theta_0,\phi_0) = \frac{1}{4\pi}\int_0^{2\pi}\int_0^{\pi} G(\theta,\theta_0,\phi,\phi_0)\,T_B(\theta,\phi)\sin\theta\, d\theta\, d\phi \tag{6}$$

The brilliance temperature distribution, obtained from data in [8], is given in the plot on the right side of Fig. 4 and it is assumed to be a function of the elevation angle (θ) only .

As a consequence, also the generic formula in (6) can be simplified as

$$T_a'(\theta_0) = \frac{1}{4\pi}\int_0^{2\pi}\int_0^{\pi} G(\theta,\theta_0,\phi)\,T_B(\theta)\sin\theta\, d\theta\, d\phi \tag{7}$$

The vertex room contribution to the antenna temperature is calculated with the same formula as in (7), by noticing that the vertex room brilliance temperature can be assumed uniform at T_{B_BWG} = 290K and taking care that the gain function is the feed gain G_F and that the integral is taken outside M4 (25° < θ < 180°).

To evaluate this contribution, the spillover efficiency of M4 illuminated by the feed (the fraction of power radiated by the feed and intercepted by the mirror M4) is introduced as

$$\eta_4 = \frac{1}{4\pi}\int_0^{2\pi}\int_0^{\theta_F} G_F(\theta,\phi)\sin\theta\, d\,\theta\, d\,\phi \tag{8}$$

where for M4 $\theta_F = 25°$.

The vertex room contribution to the antenna temperature is thus given by:

$$T_{BWG} = T_{B\_BWG}(1-\eta_4) = 290(1-\eta_4)[K] \tag{9}$$

and it has to be noticed that it is mainly a function of the vertex room temperature and the edge taper of the feed on M4. It has also to be noticed that the antenna temperature contribution in the range $20° < \theta < 25°$ (in the feed system reference) comes from the spillover of the secondary mirror M2. This effect is taken into account in the electromagnetic model of the antenna and associated to the sky and earth contributions as described above.

From (7) and (9) it is thus possible to finally calculate the overall system temperature (5) and the antenna temperature:

$$T_a = T_a'(\theta_0) + T_{BWG} \tag{10}$$

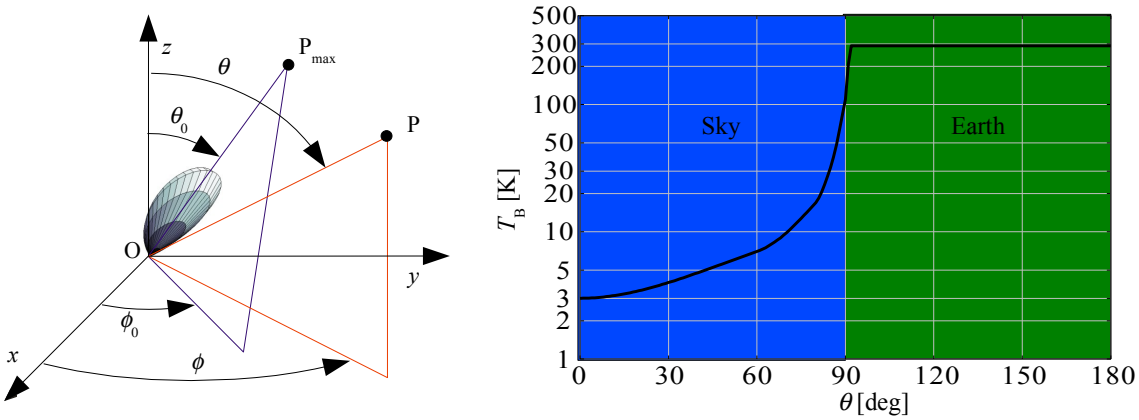

Fig. 4: Reference for the evaluation of the sky and earth temperature (left). Brilliance temperature function (right).

4 Feed design

To evaluate the G/T_{sys} merit figure, the beam pattern of the SRT has been calculated, taking into account the full electromagnetic model of the four mirrors. In the analysis a total of 17 circular corrugated horns have been used as parameter, on purpose designed to provide 1dB stepped edge tapers in the range from 9dB to 25dB. The edge taper represents the on-axis field with respect to the field at the mirror edge, corresponding to 20deg from the feed axis.

To have an idea of the dimension of each feed, the plot in Fig. 5 shows the aperture diameter versus the feed length. The shortest feed (about 65cm) provides 9dB tapering while the 24dB taper feed is the longest one (about 1m). The shortest diameter (about 17cm) is associated to 9dB taper again and the largest (about 24cm) to 25dB.

All the feeds show the same basic behaviour along the bandwidth about input matching and cross-polarization. To summarize this, the plots in Fig. 6 show for each feed, characterized by its taper, the range of the values occurred in the 5.7-7.7GHz band of both the input reflection coefficient and the maximum of cross-polarization (on the 45°-plane beam pattern cut). For each curve, the minimum, the maximum and the mean values are pointed out. It has to be highlighted no sensitive differences among the horns as regards these features.

The phase center location of the horns is given in Fig. 7.

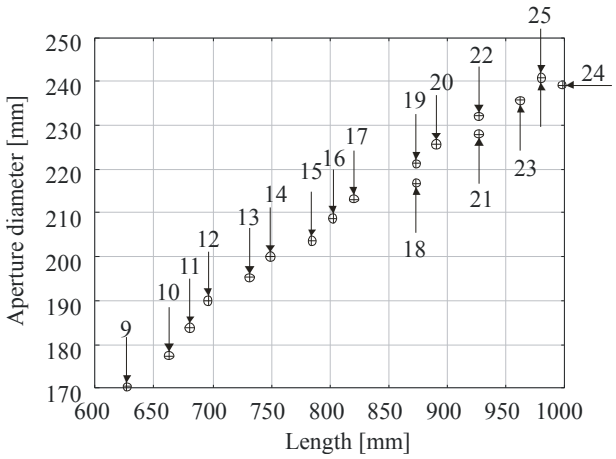

Fig. 5: Size of the feeds used for the edge taper parametric analysis.

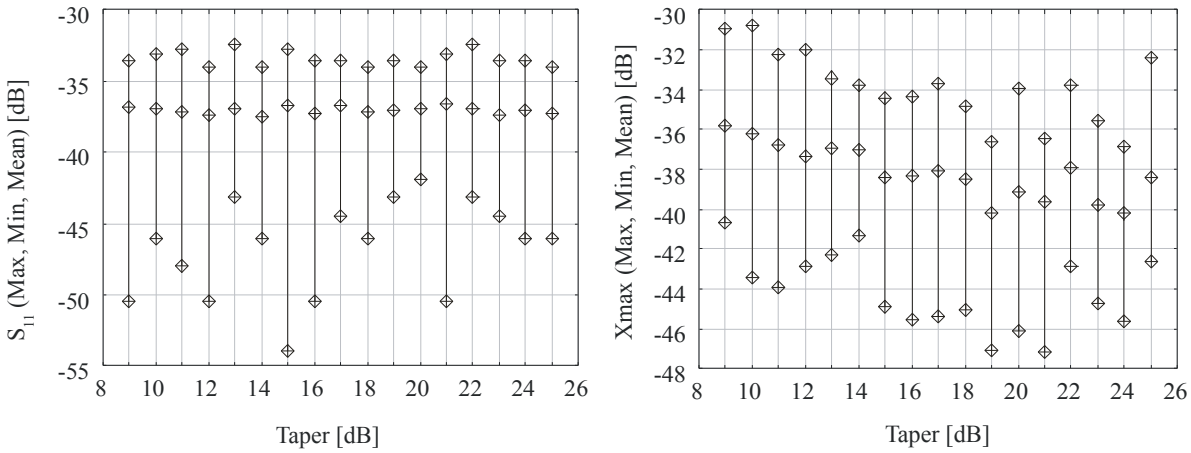

Fig. 6: Reflection coefficient (left) and cross-polarization maximum (right) of the 17 horns.

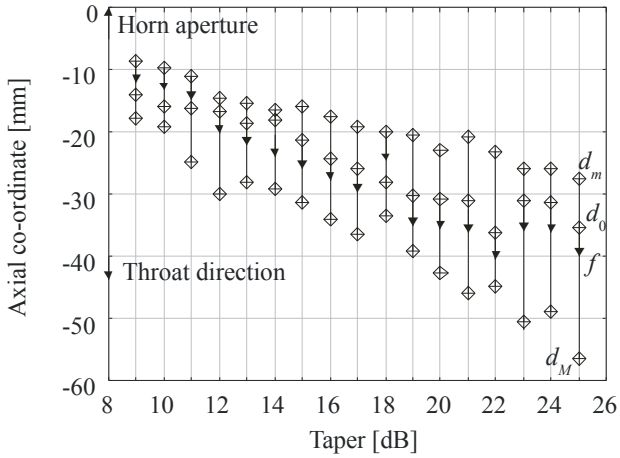

Fig. 7: Phase center location in the frequency band of the 17 horns.

The plot in Fig. 7 gives the axial co-ordinate (the origin is the horn aperture) of the phase center of each horn characterized by its taper value on the abscissa. The phase center ranges from a minimum distance d_m, at the lower frequency edge (5.7GHz), to a maximum distance d_M, at the upper frequency edge (7.7GHz): the center frequency (6.7GHz) point d_0, is also evidenced. The phase center position spread over the bandwidth slightly increases with taper.

The electromagnetic coupling of each feed with the mirrors has been accurately modelled and the gain at the 6.7GHz central frequency of the bandwidth has been calculated and plotted in Fig. 8.

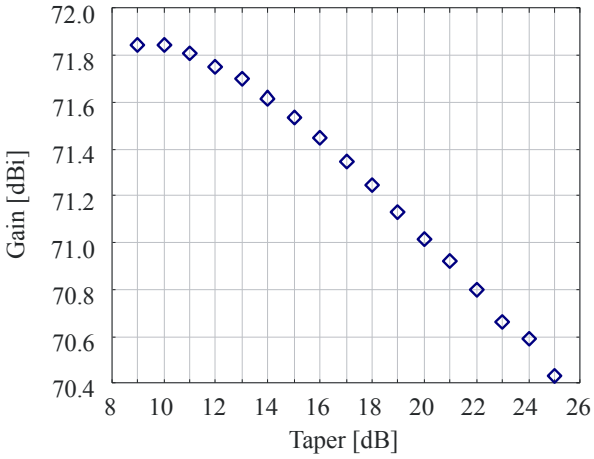

Fig. 8: SRT antenna gain versus the feed taper.

The gain analysis takes into account the two major contributions to the antenna efficiency, that is illumination and spillover; in this case the shaped configuration of both the primary and the secondary mirror minimizes the secondary mirror blockage effects, resulting in a negligible contribution to the overall efficiency.

According to (7) the sky and the earth contributions to the antenna temperature are then calculated and the results are given in the plots of Fig. 9. The sky contribution is a function dominated by the elevation angle and practically not influenced by the feed taper (Fig. 9a).

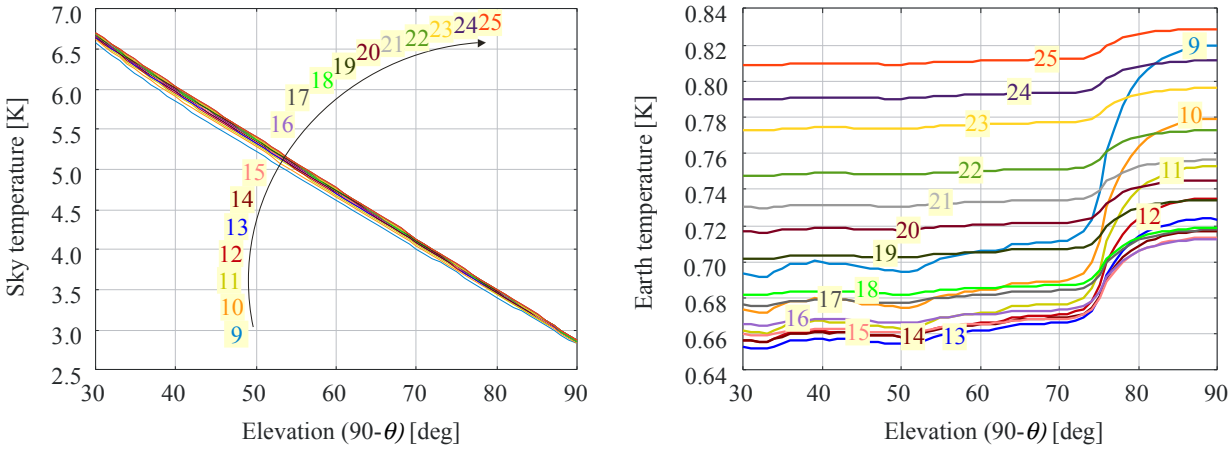

Fig. 9: Antenna temperature: Sky (a) and Earth (b) contributions parametrized to the feed taper.

The same conclusion does also hold for the earth contribution, about an order of magnitude less than the sky contribution (Fig. 9b). Although the earth doesn't give any significant contribution to the antenna temperature, it is

interest to notice that in the taper range between 13dB and 25dB the earth contribution increases with the taper, since the taper increment gives lower gains (and broader beams) and, in percentage, more energy is received from even far side lobes. Below 13dB, the (still not significant) raising trend of the low taper curves, especially close to the zenithal angle ($\theta = 0$) is due to greater diffraction effects due to higher field levels at the secondary mirror edges.

From (8) and (9) it is possible to calculate the vertex room contribution to the antenna temperature and the results are given in Fig. 10. In this case the BWG temperature is independent on the elevation angle, being a function of the feed taper only.

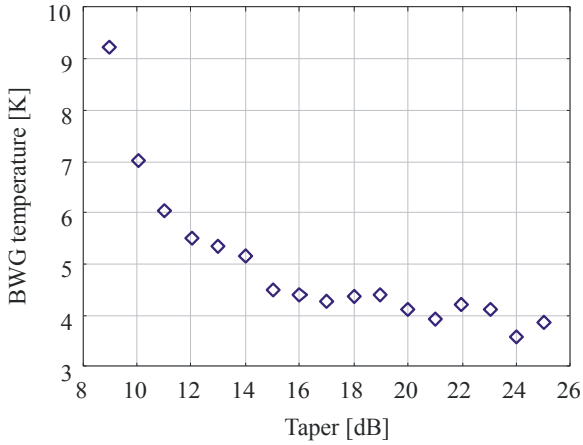

Fig. 10: Antenna temperature: BWG contribution versus the feed taper

Comparing the plots in Fig. 9 and Fig. 10, it is noticed that the sky and the BWG equally give the major contribution to the antenna temperature around 5K; while, however, the sky contribution is basically a function of the elevation angle, the BWG contribution is affected by the feed taper only.

As a result, the overall antenna temperature (10) is given in Fig. 11.

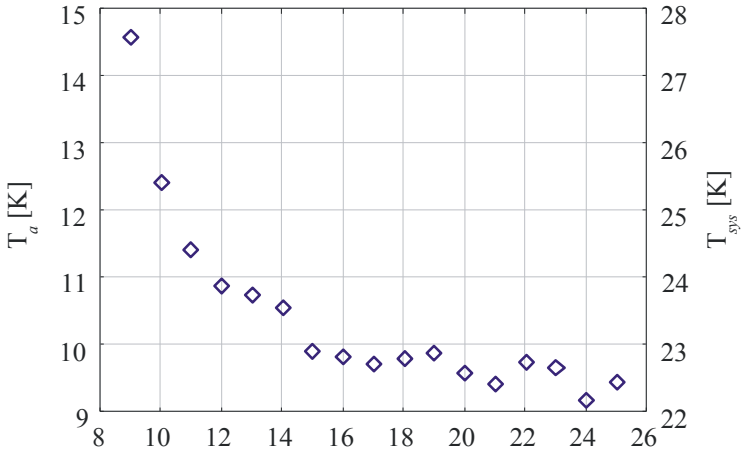

Fig. 11: Antenna temperature (left scale) and system temperature (right scale) at 6.7GHz.

It is assumed that the receiver temperature is about 13K all over the bandwidth and thus the shape of the system temperature curve is the same as the antenna temperature curve. This last is given on the right scale in Fig. 11.

All the data required to estimate the antenna gain over system temperature merit figure are already presented. It is thus possible now to synthesize the plots in Fig. 8 and Fig. 11 to have the G/T_{sys} curve.

It is interest to show both the G/T_{sys} and G/T_a curves to better appreciate how important the receiver contribution is; this is done in Fig. 12 at 6.7GHz as a function of the feed taper.

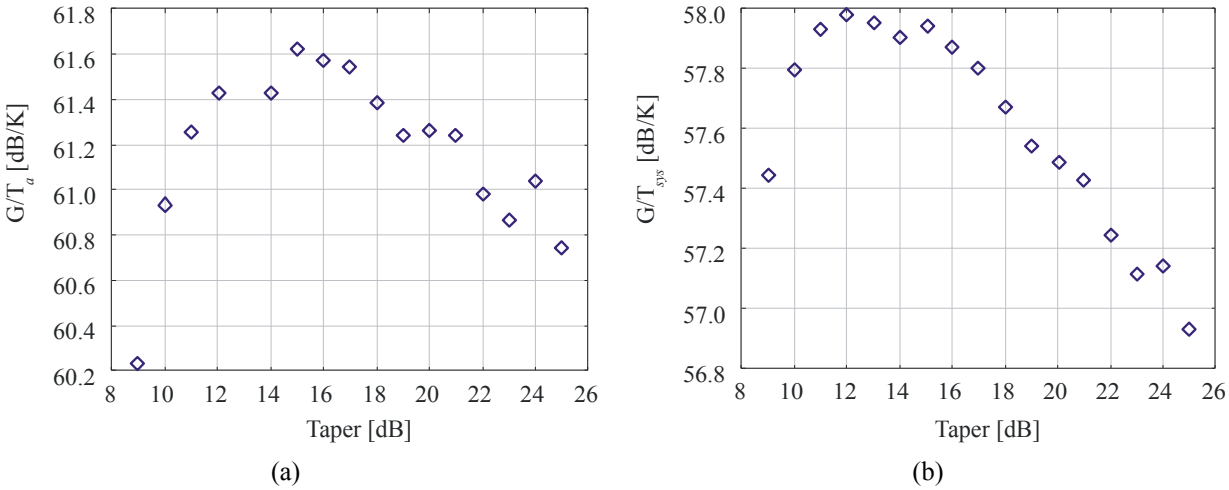

(a) (b)

Fig. 12: Merit figure: gain over antenna temperature (a); gain over system temperature (b).

5 Feed fabrication

Optimizing the G/T_{sys} merit figure at 6.7GHz, the 12dB taper feed has been thus chosen to be fabricated for the SRT optics. Furthermore, since the receiver has been scheduled to be tested on the Cassegrain focus of the Medicina radio telescope, a corrugated extension has been designed to accommodate for this different optics (see Table I). Based on studies at 22GHz [5], 9dB taper to the secondary mirror edges has been adopted as specification to be provided by the resulting feed when the extension (named MED part) is attached to the base feed (named SRT part, Fig. 13).

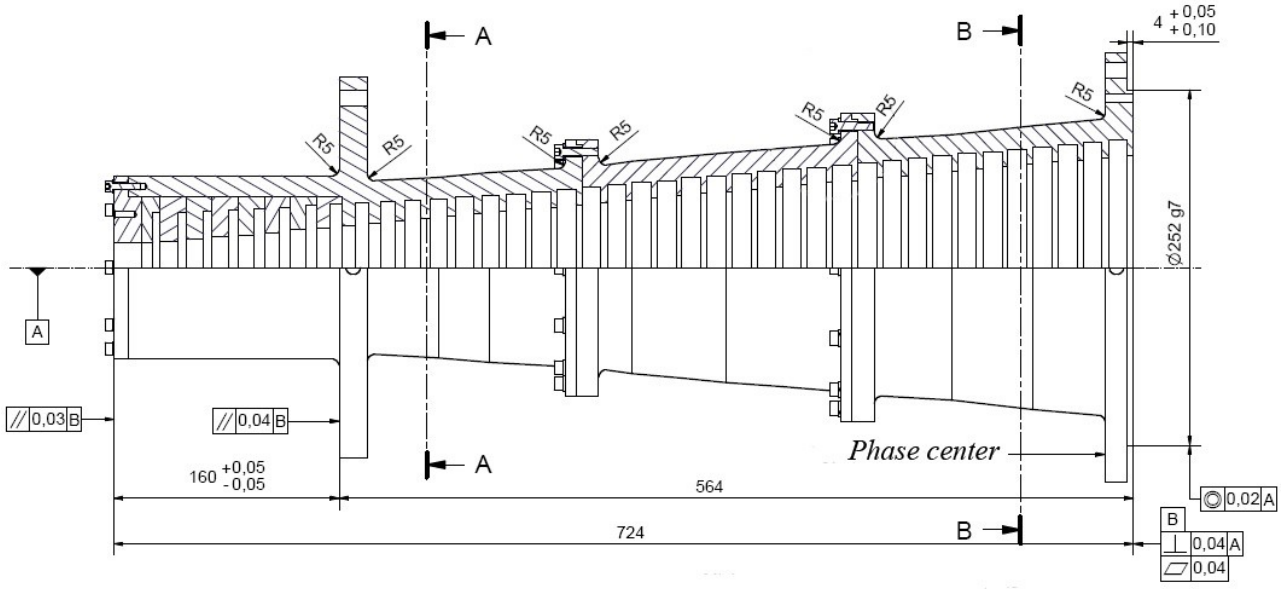

Fig. 13: Drawing of the SRT feed providing 12dB taper at 20deg half angle.

The drawing of the MED part, designed to be directly attached to the SRT feed aperture, is shown in Fig. 14.

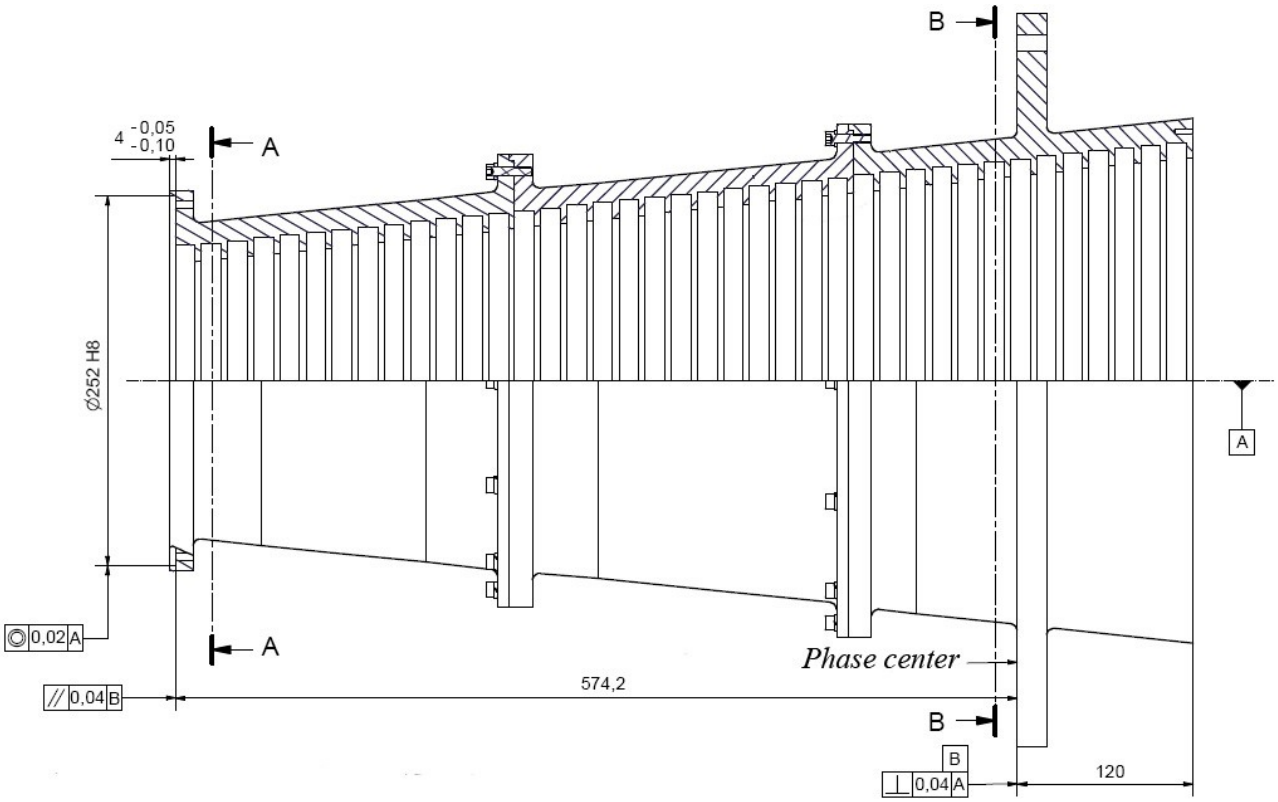

Fig. 14: Drawing of the MED part. When attached to the SRT feed provides 9dB taper at 9.5deg half angle.

Both the SRT feed and the MED part extension are fabricated in three pieces for easy machining. Finally, to ensure good electrical properties, an alodine treatment has been done on the surface.

6 Feed Test

The reflection coefficient of the feeds have been measured indoor (Fig. 15), using an Anritsu 37277C vector network analyzer, calibrated to output directly the mismatch of the feed.

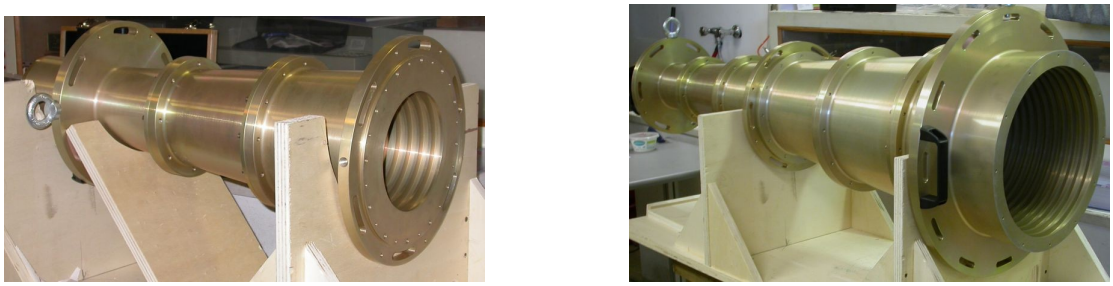

(a) (b)

Fig. 15: Corrugated feeds under test. SRT (a) and SRT+MED (b).

To reproduce as much as possible the free space load condition of the operative feed environment and avoiding spurious reflections of Lab objects, electromagnetic absorbing material panels has been properly placed nearby the feed aperture. Results of measurements are given in Fig 16, showing very good agreement with expected data and highlighting return loss performances always better than 30dB in the whole 5.7-7.7GHz operative band.

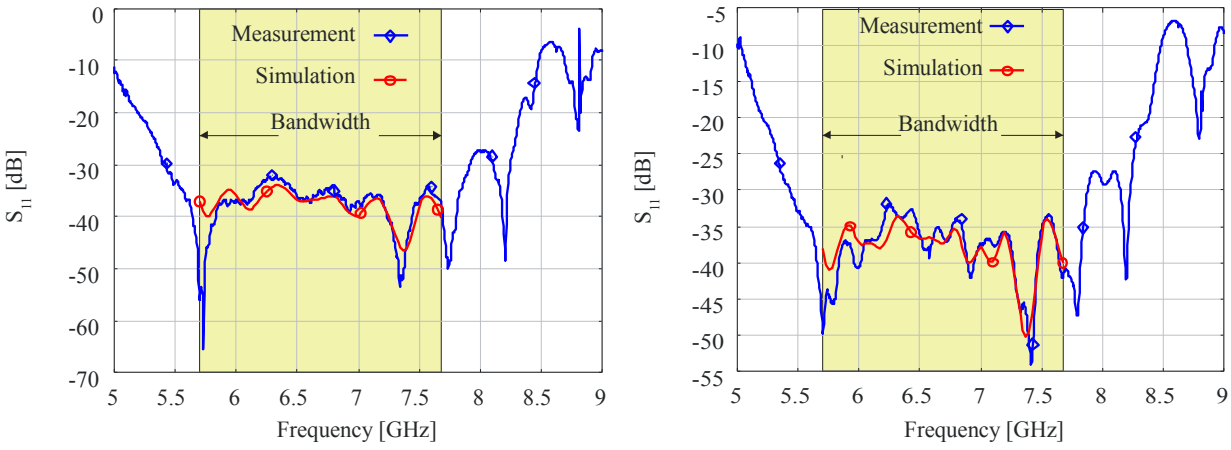

Fig. 16: Reflection coefficients of the corrugated feeds. SRT (a) and SRT+MED (b).

The return loss is better than 30dB in the whole 5.7-7.7GHz operative band.

In exactly the same configuration, except for the loading of the radiating aperture, the transmission coefficient has been determined by measuring the S_{11} scattering coefficient. In this case the radiating aperture has been short-circuited with a conductive plate place on it, and S_{11} gives the horn transmission coefficient doubled. The results for the one-way transmission measurement of both the SRT and SRT+MED horns are given in Fig. 17.

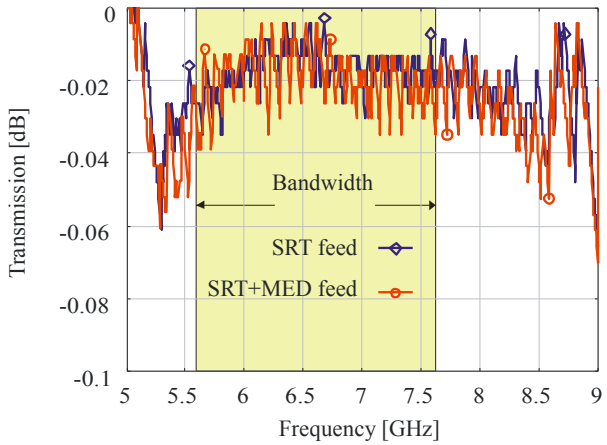

Fig. 17: Transmission coefficient of both the SRT and SRT+MED corrugated feed.

The ripples in the curves of Fig. 17 are due to the adopted measurement method. By short circuiting the radiating aperture a resonant cavity is created for all those modes which are under cut-off at the feeding waveguide, and the ripples are the evidence of these resonances. These effects seem to produce in the measurement an uncertainty of about 0.02dB, approximately the height of the ripples, but, since resonances add spurious contributions to losses, the upper

envelope of the curves is assumed a good estimate of the one-way horn transmission, thus lying between 0.01-0.02dB in the bandwidth.

The test on the pattern has been done outdoors, exploiting the suitable shape of the beautiful hills around the Arcetri Observatory (Fig 18).

Receiver Transmitter

Fig. 18: Facilities and environment for the test on the feed pattern.

A large terrace has been used to locate the feed under test and the receiving instrumentation, having reasonable easy access to power sockets. The transmitter consists of 60cm paraboloidal dish illuminated by a WR134 standard waveguide directly fed by an Anritsu signal generator. The power to the transmitter has been provided by a car battery through an inverter. The main parameters of the electromagnetic link between transmitter and receiver are summarized in Table II.

Table II

Parameters of the electromagnetic link between transmitter and receiver			
Parameter	**Value**		
Frequency GHz	5.70	6.70	7.70
Signal generator power transmitted [dBm]	10.00	10.00	10.00
Transmitter Gain (ε =0.81, estimated) [dB]	30.16	31.57	32.77
Feed Gain (SRT; SRT+MED) [dB]	18.01; 23.43	19.43; 24.91	20.72; 25.94
Path Loss (220m)[dB]	94.40	95.81	97.02
Horn Throat Receiving Power (SRT; SRT+MED) [dBm]	-36.23; -30.81	-34.81; -29.33	-33.52; -28.30

Taking advantage of a smooth shaped green depression between the transmitter and the receiver, the operative environment did not present noticeable multipath effects.

To optimize the dynamic range of the measurement a low noise amplifier and a 3MHz bandwidth filter have been used. The receiving horn was placed on a digitally controlled turntable to simultaneously acquire both the angular position and the power received and consequently record both the E and the H plane patterns of both the SRT and the SRT+MED feed at the frequency of 5.7, 6.7, 7.7GHz.

From the E and H plane pattern measurements, the 45° plane cross-polar pattern has been evaluated according to formulas given in [1]. This indirect measurement of the cross-polar pattern gives more accuracy than the direct measurement on the 45° plane, due to the practical difficulties to achieve the required precision in the alignment.

The measured patterns are compared with simulations in Figg. 19-27 showing very good agreement between them. The environmental scattering and the receiver noise allows good comparison up to about 35-40dB down the maximum for all of the frequencies. It has to be noticed that the left part of all the plots are more noisy and this really corresponded to a worse environment in that direction producing spurious electromagnetic scattering, but these effects are however negligible as regards the main lobe.

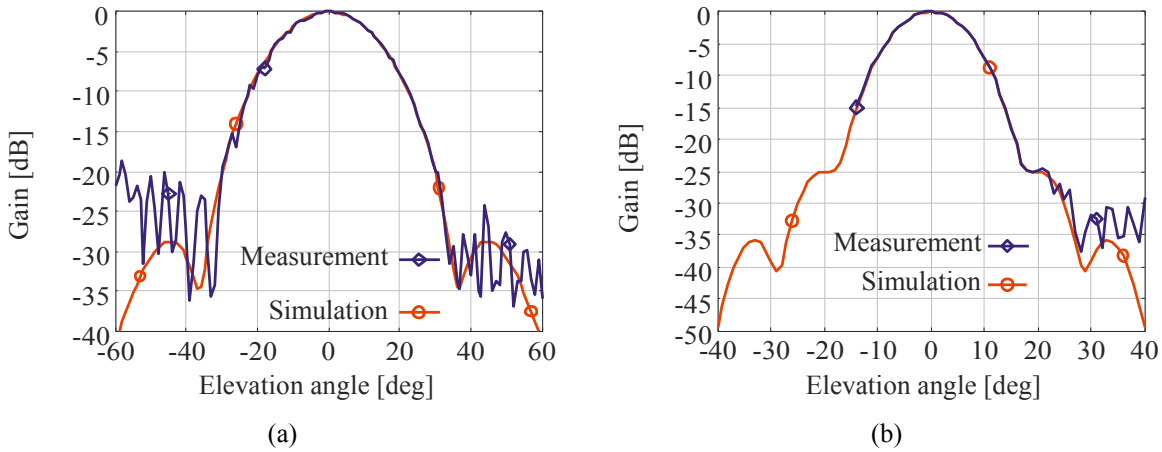

Fig. 19: Copolar E-plane patterns at 5.7GHz: SRT feed (a) and SRT+MED feed (b).

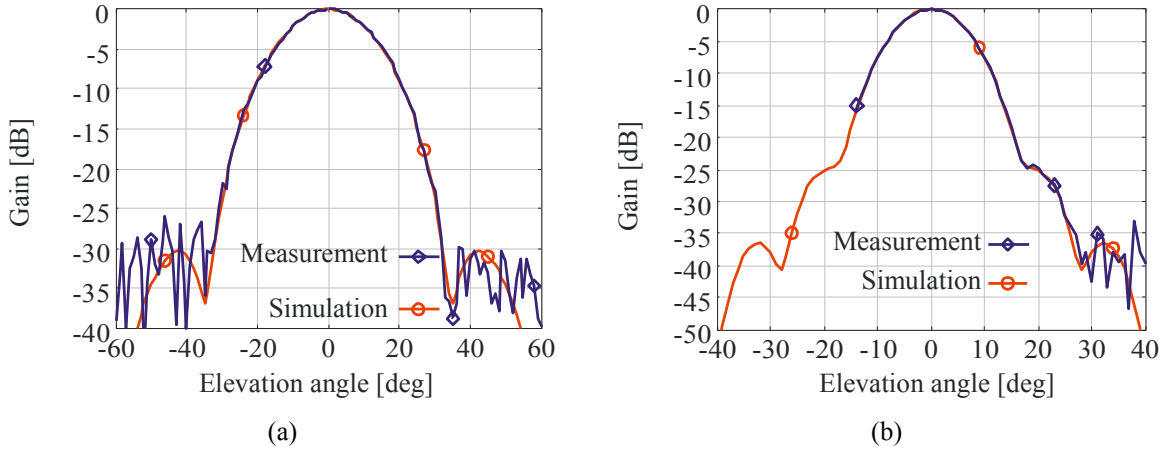

Fig. 20: Copolar H-plane patterns at 5.7GHz: SRT feed (a) and SRT+MED feed (b).

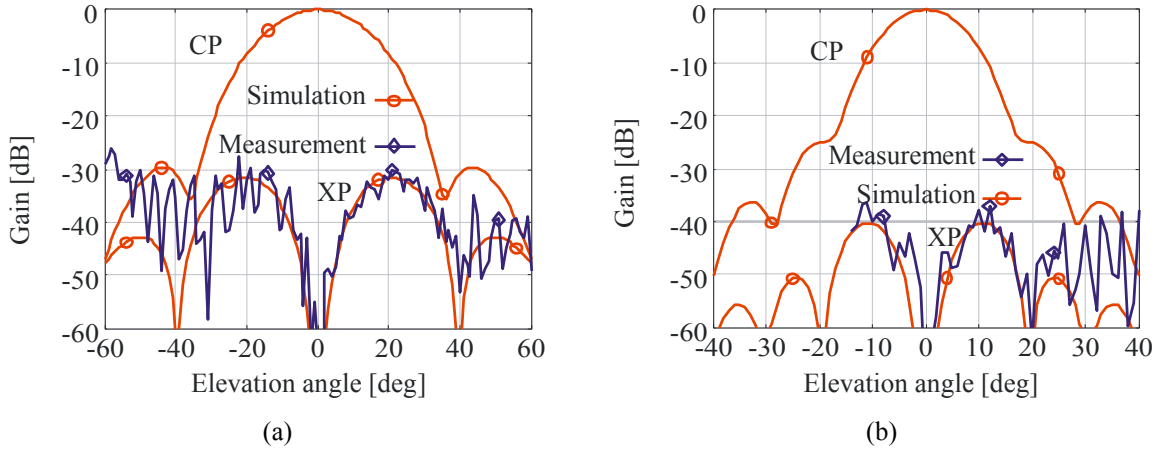

Fig. 21: Cross-polar (XP) and copolar (CP) 45°-plane patterns at 5.7GHz: SRT feed (a) and SRT+MED feed (b).

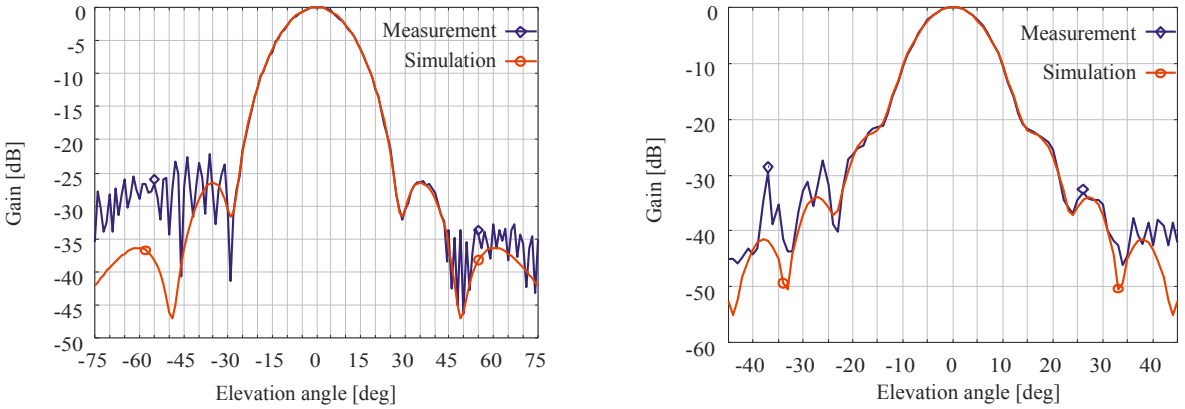

Fig. 22: Copolar E-plane patterns at 6.7GHz: SRT feed (a) and SRT+MED feed (b).

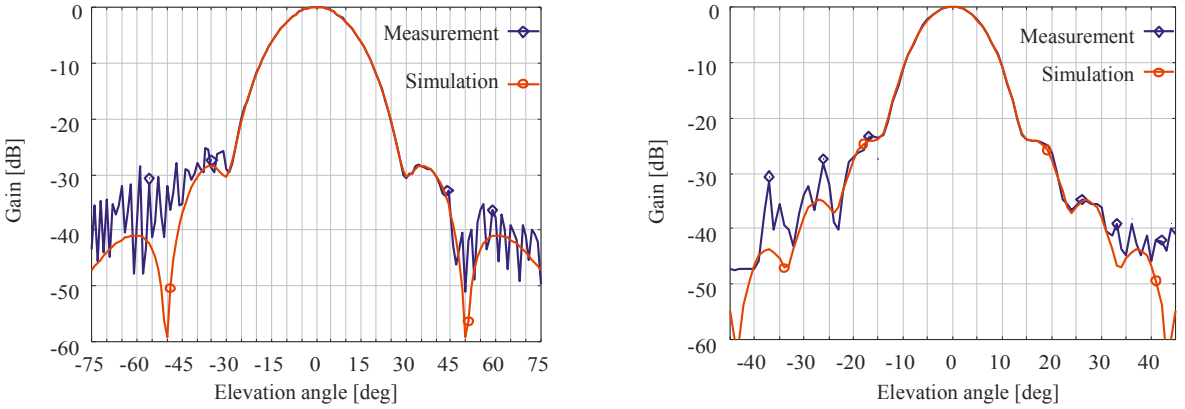

Fig. 23: Copolar H-plane patterns at 6.7GHz: SRT feed (a) and SRT+MED feed (b).

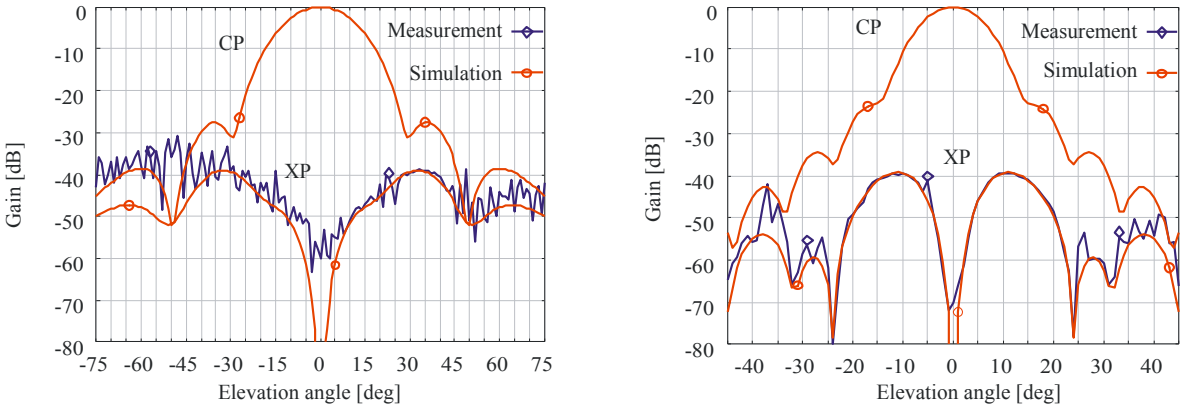

Fig. 24: Cross-polar (XP) and copolar (CP) 45°-plane patterns at 6.7GHz: SRT feed (a) and SRT+MED feed (b).

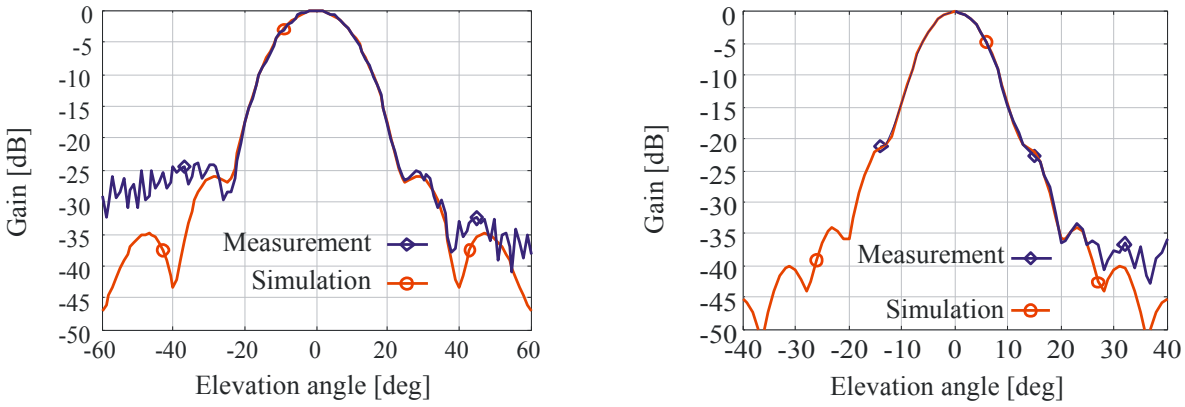

Fig. 25: Copolar E-plane patterns at 7.7GHz: SRT feed (a) and SRT+MED feed (b).

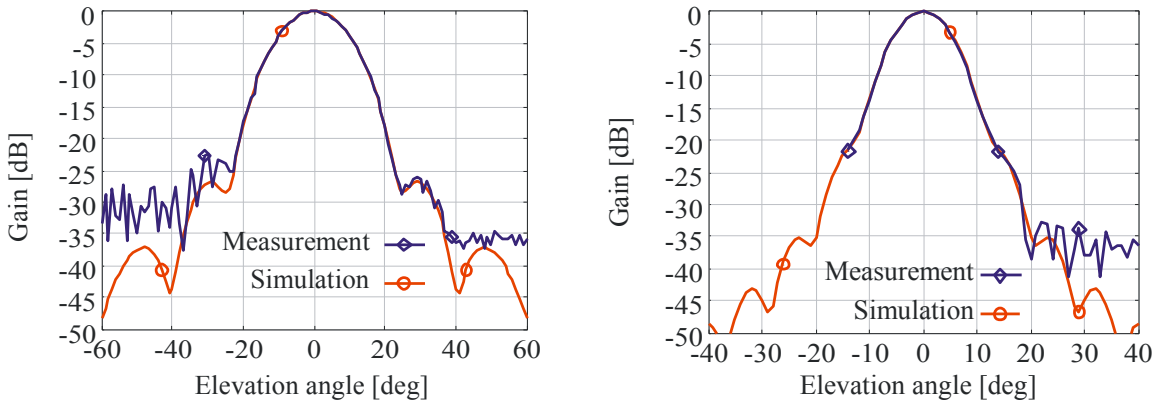

Fig. 26: Copolar H-plane patterns at 7.7GHz: SRT feed (a) and SRT+MED feed (b).

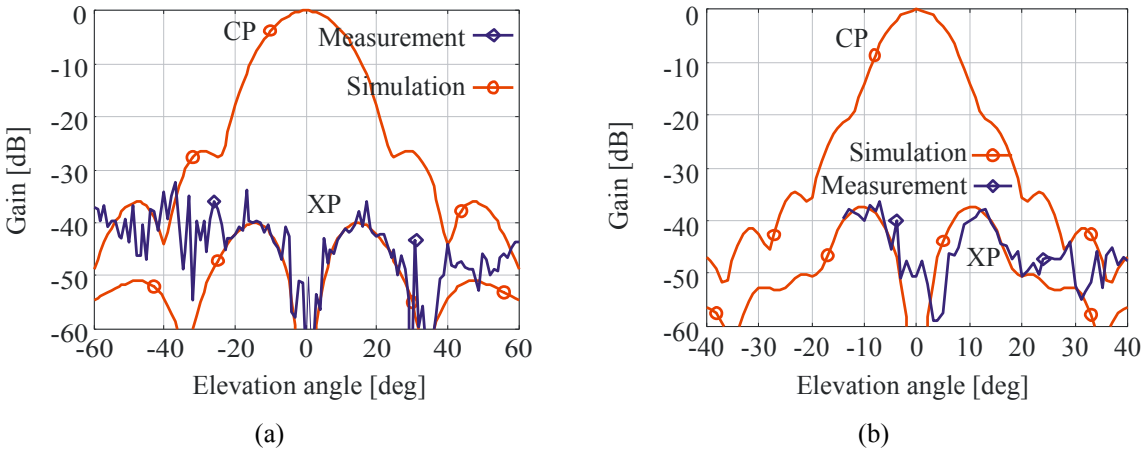

Fig. 27: Cross-polar (XP) and copolar (CP) 45°-plane patterns at 7.7GHz: SRT feed (a) and SRT+MED feed (b).

Appendices

A-I Geometrical properties of practical reflector system configurations

One of the most broad band concepts in the technological world of Optics is the *focal ratio*, which is used to characterize photon guide systems, ranging from radio wave reflector antennas to optical devices like telescopes and cameras. Its usefulness comes from its ability to summarize the features of complex optical systems, with an arbitrary number of scatterers, in terms of a simple dimensionless number which is the ratio between two intuitive distances, an *effective focal length* and an *effective aperture diameter* giving at the same time a simple way to take into account the coupling between the optics and the feed system. With reference to radio astronomy applications, the *focal ratio* approach is here used in the description of classical reflector antennas, such as the simple paraboloidal reflector, the Cassegrain and Gregorian dual reflector systems, and advanced configurations involving more re-focusing elements. Some not so popular geometrical properties of conics are also evidenced.

The *focal ratio* is properly defined for the base reflector antenna, that is the paraboloid, characterized by the *aperture diameter D* and the *focal length F*, which is the distance between the focus and the paraboloidal vertex: the *focal ratio* is simply defined as the dimensionless ratio *F*/*D*. In practice a paraboloidal mirror is illuminated by a feed placed at its focus and the resulting system is described introducing one more parameter: the angular region subtended by the reflector, as seen by the feed. This solid angle region is, in most practical systems, formed by an azimuthal rotation of a linear angle which is taken as the characteristic parameter of the feed-reflector coupling and named *taper angle* Ψ. All of these features are sketched in Fig. 28.

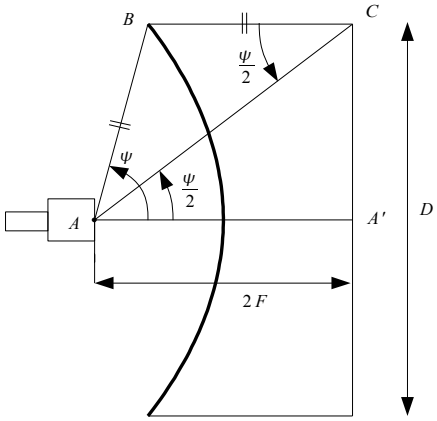

Fig. 28: Geometrical parameters of a paraboloidal reflector fed from its focus.

In a paraboloidal antenna, it can be demonstrated that the three parameters *F*, *D* and Ψ, are simply related. From Fig. 28, observing that the triangle *ABC* is isosceles since *AB* and *BC* are the equal distances from a point on the parabola to, respectively, the focus and the directrix, it is possible to conclude that the angles $\widehat{CAB}=\widehat{BCA}$. Since *AA′* and *BC* are parallel, it follows that also the angles $\widehat{A'AC}=\widehat{BCA}$. Since $\psi=\widehat{A'AB}$ it follows:

$$\widehat{CAB}=\widehat{A'AC}=\frac{\psi}{2} \tag{11}$$

The ratio of the sides *A′C* and *AA′* of the right-angle triangle *A′AC* can thus be written as:

$$\tan\left(\frac{\psi}{2}\right)=\frac{D}{4F} \tag{12}$$

The above equation is a simple relation about the geometrical parameters of a paraboloidal reflector and the way it is seen by a feed on its focus. It has to be noticed that the equation basically relates the taper angle and the focal ratio, since it is possible to derive:

$$F/D=\frac{1}{4\tan(\frac{\psi}{2})}=\frac{1}{4}\cot(\frac{\psi}{2}) \tag{13}$$

It is possible to go further this way, extending this formalism to the description of multireflector systems as shown in the following.

A-II Focal length properties of the ellipsis and the hyperbola

Besides the paraboloid, three other types of mirrors are largely used in reflector antenna systems: the flat mirror, the ellipsoid and the hyperboloid. The flat mirror simply behaves like a mirror and basically doesn't affect the optical properties of the antenna. Both the ellipsoid and the hyperboloid produce instead a sensitive modification of the antenna features since they change, like paraboloids do, the radius of curvature of the phase front of the incident electromagnetic wave. In practice, given a paraboloidal mirror, one or more of them are used to synthesize a different paraboloid [4], acting as a sort of *focal length* transformer.

The above properties are related to the geometrical properties of the ellipsis and hyperbola These properties are not so popular and thus we find useful to show them in some detail.

Consider for example the ellipsis in Fig. 29a. It is quite well known that the sum of the distances of an arbitrary point P on the ellipsis from the two foci C_1 and C_2 is constant and equal to major axis. This obviously holds also for the point V which is here considered as the vertex of the ellipsis: in this case the distances are indicated as F_1 and F_2 and are considered as the two *focal lengths* of the curve.

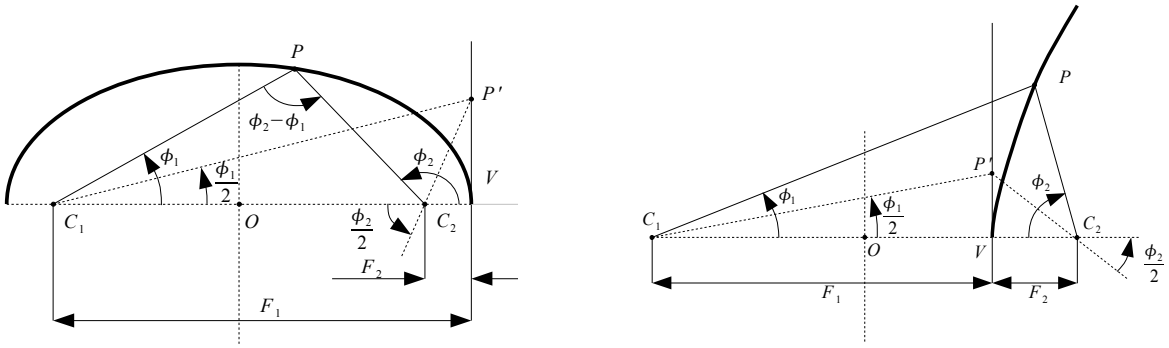

(a) (b)

Fig. 29: Some geometrical parameters of an ellipsis and an hyperbola.

A very interesting property from our point of view, is the not well known and quite unintuitive fact that the bisectors of the angles subtended by the arc PV, with vertex in the two foci, intersects on a point P' on the line tangent in V to the ellipsis. Using formulas, this property can be expressed as:

$$F_1\tan(\frac{\phi_1}{2})=F_2\tan(\frac{\phi_2}{2}) \tag{14}$$

In the case of the ellipsis, to demonstrate (14) it is possible to apply the sine law to the triangle PC_1C_2 leading to:

$$\frac{F_1-F_2}{\sin(\phi_2-\phi_1)}=\frac{F_1+F_2-PC_1}{\sin(\phi_1)}=\frac{PC_1}{\sin(\pi-\phi_2)}=\frac{PC_1}{\sin(\phi_2)} \tag{15}$$

Eliminating PC_1 from the expression II and IV in (15) it is found:

$$\frac{PC_1}{\sin(\phi_2)}=\frac{F_1+F_2}{\sin(\phi_2)+\sin(\phi_1)} \tag{16}$$

and using the expression I:

$$\frac{F_1-F_2}{\sin(\phi_2-\phi_1)}=\frac{F_1+F_2}{\sin(\phi_2)+\sin(\phi_1)} \tag{17}$$

Using the following trigonometric identities:

$$\begin{cases}\sin(\phi_2-\phi_1)=2\sin(\frac{\phi_2-\phi_1}{2})\cos(\frac{\phi_2-\phi_1}{2})\\ \sin(\phi_1)+\sin(\phi_2)=2\sin(\frac{\phi_2+\phi_1}{2})\cos(\frac{\phi_2-\phi_1}{2})\end{cases} \tag{18}$$

it is possible to transform (17) as follows

$$\left(\frac{F_1}{F_2}-1\right)\sin\left(\frac{\phi_2+\phi_1}{2}\right)=\left(\frac{F_1}{F_2}+1\right)\sin\left(\frac{\phi_2-\phi_1}{2}\right) \tag{19}$$

and finally

$$\frac{F_1}{F_2}=\frac{\sin\left(\frac{\phi_2+\phi_1}{2}\right)+\sin\left(\frac{\phi_2+\phi_1}{2}\right)}{\sin\left(\frac{\phi_2+\phi_1}{2}\right)+\sin\left(\frac{\phi_2+\phi_1}{2}\right)}=\frac{\sin\left(\frac{\phi_2}{2}\right)\cos\left(\frac{\phi_1}{2}\right)}{\sin\left(\frac{\phi_1}{2}\right)\cos\left(\frac{\phi_2}{2}\right)}=\frac{\tan\left(\frac{\phi_2}{2}\right)}{\tan\left(\frac{\phi_1}{2}\right)} \tag{20}$$

Exactly the same equation (14) holds for the analogous parameters of the hyperbola in Fig. 29b. In this case it is constant the difference between the two distances of an arbitrary point P on the hyperbola to its foci C_1 and C_2, which can be expressed as F_1 - F_2; the application of the sine law to the triangle PC_1C_2 leads to:

$$\frac{F_1+F_2}{\sin(\phi_2+\phi_1)}=\frac{PC_1-(F_2-F_1)}{\sin(\phi_1)}=\frac{PC_1}{\sin(\pi-\phi_2)}=\frac{PC_1}{\sin(\phi_2)} \tag{21}$$

and the same procedure, as used in the ellipsis case, leads to (14).

Eq. (14) can be considered as the final result of this appendix, since it represents the main reference law used in [4] in describing the concept of the equivalent parabola and the relation between taper angles and focal lengths of multi-reflector optical systems.

References

[1] P. J. B. Clarricoats, A. D. Olver, *Corrugated Horns for Microwave Antennas*, Peter Peregrinus Ltd, London, 1984.
[2] http://www.srt.inaf.it/
[3] http://www.med.ira.inaf.it/parabola_page_EN.htm
[4] Hannan, P. W., "Microwave Antennas Derived from the Cassegrain Telescope," *WIRE Trans. Antennas Propagat.* Vol. 9, n. 2, pp. 140-153, 1961.
[5] R. Nesti, "Optimum feed taper value for the 18-26GHz multifeed system", INAF SRT-Project, GAI04 Memo Series n. GAI04-TM-8.0, Apr. 2005.
[6] W. L. Stutzman, G. A. Thiele, *Antenna theory and design*, Wiley, New York, 1998.
[7] J. D. Kraus, *Radio Astronomy*, McGraw-Hill, New York, 1966.
[8] G. Cortés Medellín, "Antenna Noise Temperature Calculations," SKA Technical Memo Series, *National Astronomy and Atmospheric Center, Cornell University*, Ithaca, NY, October 20, 2004.